

CHAPTER 3

Observations and Data Analysis

The Hubble Space Telescope (HST), as seen in Figure 3.1 was designed for high resolution observations of outer planets, stars and galaxies. The HST was sponsored by the National Aeronautics and Space Administration (NASA) and contributions from the European Space Agency (ESA). HST is operated by the Space Telescope Science Institute (STSCI). HST has a 2.4 m primary mirror, with length: 13.2 m, and additional two solar panels of 2.45 x 7.56 m.

Observations of Jupiter's auroral emission in this study had been using two instruments, the Space Telescope Imaging Spectrograph (STIS) and Advanced Camera for Surveys (ACS), which were installed onboard HST. STIS was used originally until broke down in 2004. Afterward ACS was used to take Jupiter's UV images until 2007, when STIS was completely repaired. All specifications for these two instruments will be discussed separately in next sections. The reduction procedure was conducted, including with dark image subtraction, flat-field correction and instrumental geometric distortion correction at Boston University (Wannawichian et al., 2010). The newly analyzed convection factor to convert Io's footprint brightness into kilo-Rayleighs ($1\text{kR} = 10^9 \text{ photons/ cm}^2 \text{ sec sr}$ and $10\text{kR} \sim 1 \text{ mW/m}^2$) (Gustin et al., 2012) was taken into consideration.

ลิขสิทธิ์มหาวิทยาลัยเชียงใหม่
Copyright© by Chiang Mai University
All rights reserved



Figure 3.1: The Hubble Space Telescope (Jäger, 2015).

3.1 Advanced Camera for Surveys (ACS)

Hubble's ACS cover wavelengths from the far ultraviolet (FUV) to visible light. It is called third generation on Hubble instrument. As seen in Table. 3.1, ACS consists of 3 channels (1) The wide field channel (WFC) installed with CCD, which was used to study the distribution of galaxies with sensitivity $\sim 3,500 \text{ \AA} - 11,000 \text{ \AA}$. (2) The High-Resolution channel (HRC) takes detailed pictures of the inner regions of galaxies, which is installed with CCD's sensitivity $\sim 1,700 \text{ \AA} - 11,000 \text{ \AA}$. (3) Solar Blind channel focus on hot stars or planets using MAMA detector with sensitivity $\sim 1,150 \text{ \AA} - 1,700 \text{ \AA}$, the same range of auroral emission. However ACS was shut down in 2007 due to electrical failure and resumed work since 2009. Wave length sensitivities for all 3 channels are presented in Fig. 3.2.

ลิขสิทธิ์มหาวิทยาลัยเชียงใหม่
Copyright© by Chiang Mai University
All rights reserved

Table 3.1: Advanced Camera for Surveys Facts (Hopkins, 2015)

Instrument type	Camera
Field of view	202 × 202 arcseconds (Wide Field Channel, WFC) 29.1 × 26.1 arcseconds (High Resolution Channel, HRC) 34.59 × 30.8 arcseconds (Solar Blind Channel, SBC)
Detector array size	4096 × 4096 (WFC) 1024 × 1024 (HRC) 1024 × 1024 (SBC)
Wavelength range	350-1050 nm (WFC) 200-1050 nm (HRC) 115-180 nm (SBC)

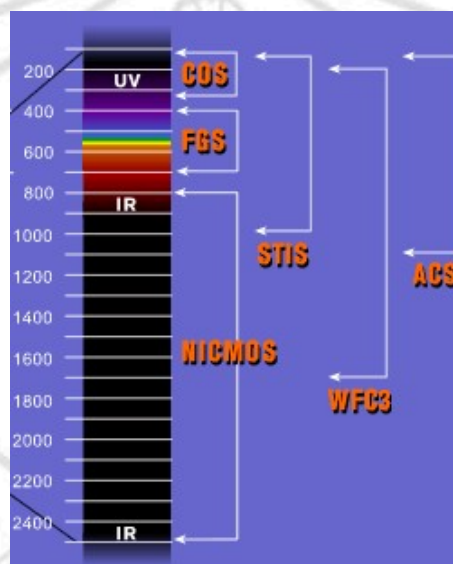


Figure 3.2: Wavelengths sensitivities in nanometers of Hubble's instruments (Hubble OPO, 2015).

3.2 Space Telescope Imaging Spectrograph (STIS)

STIS is working over ultraviolet, visible and near-infrared wavelengths. In ultraviolet (UV), STIS works in near-UV (1600 Å - 3100 Å) and in FUV (1150 Å - 1700 Å). Aurora observations use the FUV MAMA (with two function 25MAMA of clear and F25SRT of filter). STIS has electronic failure in 2004 and resumed operations with all ultraviolet and optical channels since 2009. The specification of all channels for STIS is shown in Table 3.2

Table 3.2: Space Telescope Imaging Spectrograph Facts (Jäger, 2015).

Instrument type	Camera and Spectrograph
Dimensions	$2.2 \times 0.9 \times 0.9$ m
Field of view	MAMA - 25×25 arcseconds CCD - 50×50 arcseconds
Wavelength range	115 to 1000 nm

Emission of Jupiter's aurora was observed in x-ray, UV, infrared, visible and radio wavelengths. Hydrogen atoms were excited by particles collision at jovian atmosphere resulting to Jupiter's aurora emission. The most significant emissions are the H Ly α (~ 121.6 nm), H₂ Lyman and Werner band. The region of auroral emission rotate with Jupiter's system III longitude (Jupiter magnetic period). The spectrum of Jupiter's auroral UV emission was showed in Fig. 3.3

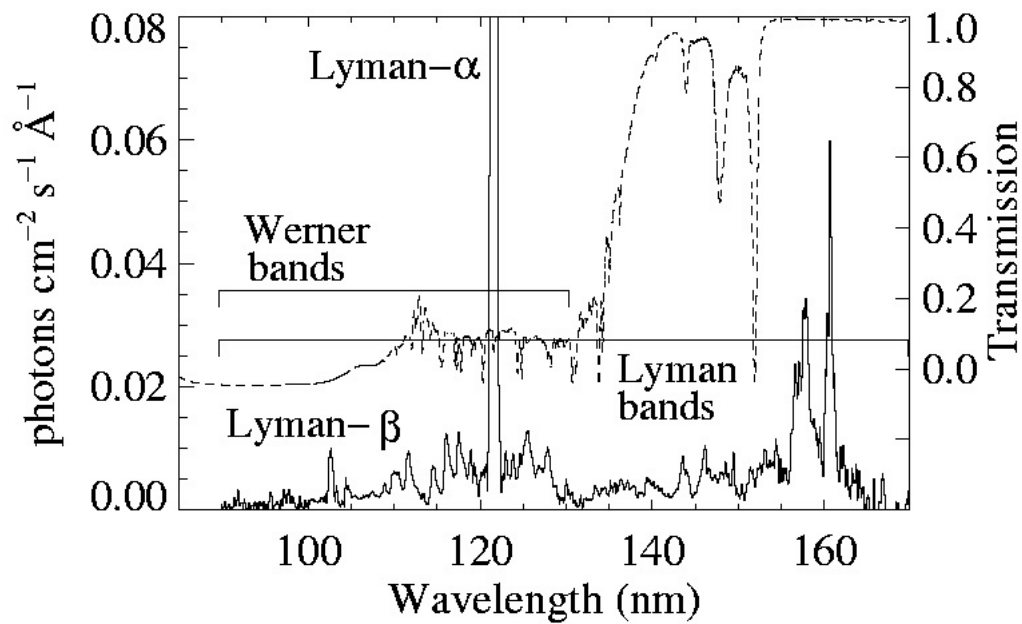


Figure 3.3: Spectrum of Jupiter's auroral UV emission (Morrissey et al., 1997).

3.3 Numerical Analysis

Images of Jupiter aurora were analyzed by Interactive Data Language program (IDL), which is a software preferably used for analyzing astronomical data, i.e. an observed auroral brightness in this study. The variation trend of Io's magnetic footprint brightness was found to have somewhat a characteristic as symmetric "bell curve". Therefore the footprint brightness variation can be analyzed by assuming a gaussian function for the distribution of the magnetic footprint brightness as a function of Io's system III longitude. The variation of Io's magnetic footprint was considered to be influenced by two plasma sources; (1) Plasma released from Io and (2) Plasma in Jupiter's magnetosphere. Those two sources would affect on the footprint brightness differently,

$$I = Ae^{-\left(\frac{\lambda_{III} - \lambda}{\sigma}\right)^2} + A_0e^{-\left(\frac{\lambda_{III} - \lambda_0}{\sigma_0}\right)^2}. \quad (3.1)$$

While I is the auroral footprint brightness at difference system III longitude (λ_{III}). σ and σ_0 are related to the Full width at Half Maximum (FWHM), which is defined as $2\sqrt{\ln 2}\sigma$. Therefor σ and σ_0 directly connect to the shape of the fitted variations. The longitude of maximum brightness (λ_0, λ) and the peak brightness of aurora will be obtained regarding to equation (3.1).

FUV auroral images from observations (Fig. 3.4) were analyzed by IDL written at Chiang Mai University. At first, a picture from observation will be cut into 100×100 pixels (Fig. 3.5), in which the Io's footprint was expected to be centralized, based on VIP4 magnetic field model (Connerney et al., 1998). Next, the brightness of Io's magnetic footprint was measured including with the subtraction of background emission. Based on Bonfond et al. (2013), the actual size of footprint would be only 1-2 pixels. Therefore only the peak brightness of each spot was calculated.

In Fig. 3.4, circular mission above Io's magnetic footprint is the main oval aurora. The center of main oval contains polar emission which is influenced by the solar wind.

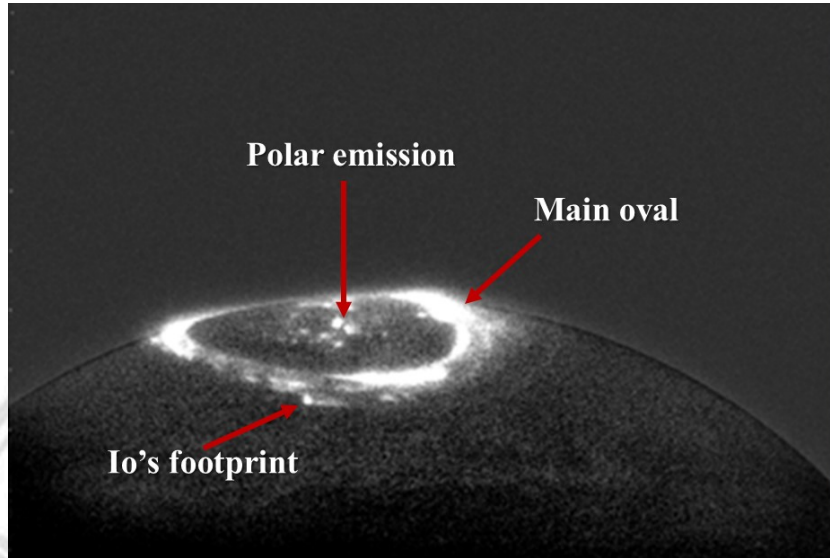


Figure 3.4: Jupiter's aurora from HST observation

The location of Io's magnetic footprint was predicted by VIP4 magnetic field model (Wannawichian et al., 2010). Within an image size of 100×100 pixels (Fig. 3.5), Io's magnetic footprint was programmed to appear at the center of picture to appear at the center of picture. This picture was analyzed for the peak brightness.

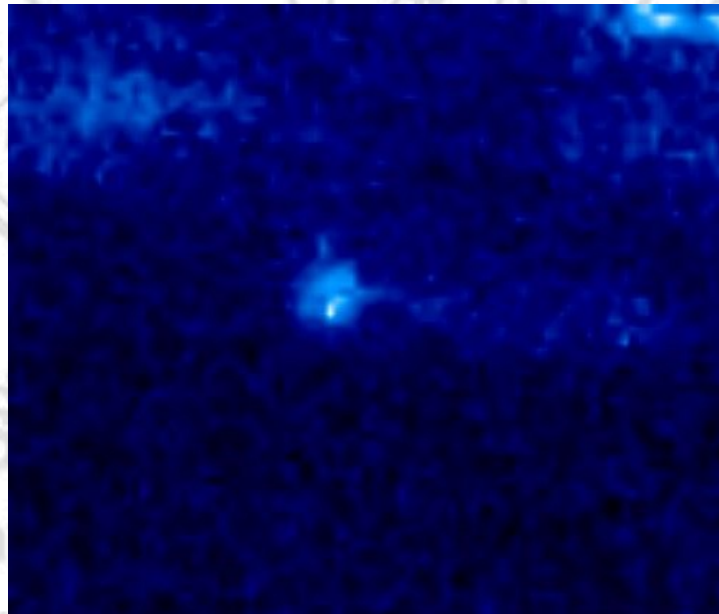


Figure 3.5: Zoomed-in image with the size of 100×100 pixel

Next step, after we have the peak brightness from observed data, the brightness variation was fitted to equation (3.1). Observed brightness for each longitude were used

for the fitted separately, for northern and southern aurora. The maximum brightness when λ_{III} equal to maximum is where $\frac{dI}{d\lambda_{III}}$ in equation (3.2) equal to zero.

$$\frac{dI}{d\lambda_{III}}|_{\lambda_{max}} = 2A \left(\frac{\lambda_{max} - \lambda}{\sigma^2} \right) e^{-\left(\frac{\lambda_{max} - \lambda}{\sigma} \right)^2} + 2A_0 \left(\frac{\lambda_{max} - \lambda_0}{\sigma_0^2} \right) e^{-\left(\frac{\lambda_{max} - \lambda_0}{\sigma_0} \right)^2}. \quad (3.2)$$

While A and A_0 is the peak brightness of each component of brightness variations. However all constant, $\lambda, \sigma, \lambda_0, \sigma_0, A$ and A_0 are obtained via numerical analysis. Therefore maximum brightness $I(\lambda_{max})$ or I_{max} can be calculated numerically.

For detail analysis, the effect of different observation times on the brightness of each longitude was compared with observed brightness. To analyze volcanic influence from Io, the brightness variation from two consecutive months were considered. In more detail, the brightness variation when Io located at the same longitude will be discussed.

The fit brightness variation of Io's magnetic footprint was divided into two main group : (1) Io's footprint brightness observed during 1997-2001 by STIS, and (2) Io's footprint brightness observed in 2007 by ACS. In 2007, observed images were separated into several months in order to analyze volcanic influence from Io on the footprint feature. The variation from month to month shows effect of volcanoes on the brightness of Io' magnetic footprint, when Io was at the same longitude. For the result, the correlation between two sets of data (for example, x and y) will be calculated as Spearman correlation (R), which is defined as;

$$R = \frac{\sum_{i=0}^{N-1} (x_i - \bar{x})(y_i - \bar{y})}{\sqrt{\sum_{i=0}^{N-1} (x_i - \bar{x})^2} \sqrt{\sum_{i=0}^{N-1} (y_i - \bar{y})^2}}. \quad (3.3)$$